Coherent nonlocal transport in quantum wires with strongly coupled electrodes

Y. Yang, G. Fedorov,* and P. Barbara†
Department of Physics, Georgetown University, Washington, DC, 20057

S. E. Shafranjuk
Department of Physics and Astronomy, Northwestern University, Evanston, Illinois, 60208, USA

B. K. Cooper, R. M. Lewis,‡ and C. J. Lobb
Department of Physics, CNAM and JQI, University of Maryland, College Park, Maryland 20742, USA
(Received 21 October 2011; revised manuscript received 26 November 2012; published 3 January 2013)

We report a one-dimensional nonlocal experiment where the conductance of a section of carbon nanotube shows regular oscillations due to phase-coherent and ballistic transport in an adjacent section. This occurs in spite of wide strongly coupled contact electrodes, which are expected to divide the nanotube into independent sections. Our simulations show that the electrodes can be modeled as shallow and wide barriers which maintain quantum coherence of electron transport between the adjacent sections for lengths of several micrometers.

DOI: 10.1103/PhysRevB.87.045403 PACS number(s): 73.63.−b, 73.23.−b

I. INTRODUCTION

When conductors are reduced to dimensions smaller than the electronic coherence length, their transport properties reveal quantum effects. A striking experiment by Umbach *et al.*[1] showed that the conductance of a gold wire was affected by an adjacent gold loop. Quantum interference of electrons traveling outside the contact probes and around the loop caused Aharonov-Bohm periodic oscillations of the conductance as a function of magnetic field, thereby unambiguously demonstrating nonlocal effects from regions outside the classical current path. However, nonlocal interference has not been observed in one-dimensional (1D) conductors. In this paper we report the observation of nonlocal coherent transport in a carbon nanotube, where the nonlocal interference pattern is obtained by continuously tuning the wavelength of electrons at the Fermi level, without applying any magnetic field.

Evidence of electrons propagating beyond a carbon nanotube (CNT) section covered by a strongly coupled electrode, such as palladium (Pd), into a neighboring section of uncovered CNT has only been seen for very narrow electrodes, just a few tens of nanometers across.[2,3] In these samples, a section of CNT was biased and a nonlocal voltage signal was measured across an adjacent unbiased section. The nonlocal voltage was due to a fraction of electrons (about 10% in Ref. 2) propagating from the biased section across the narrow electrode and into the unbiased section.

For strongly coupled materials like Pd, this nonlocal effect is widely believed to disappear when the electrode width is increased beyond a few tens of nanometers, especially for large diameter nanotubes, where high-transparency contacts can more easily be achieved due to a larger CNT/metal interface.[4,5]

Previous experimental work[6] and first-principle calculations of a CNT surrounded by Pd atoms[5] argue that strongly coupled Pd electrodes divide the nanotubes into independent sections and that the current of the nanotube segment underneath the Pd electrode is basically shunted through the Pd.

In contrast to this picture, we show that even in the case of large and strongly coupled contacts and large-diameter nanotubes, a significant fraction (higher than 10%) of electrons propagate across the electrode, causing phase-coherent nonlocal transport extending a few micrometers beyond the electrode.

II. EXPERIMENTS AND RESULTS

Our sample is a semiconducting CNT with multiple Pd electrodes, as shown in Fig. 1(a). The electrodes are 650 nm wide and 50 nm thick. The lengths of the CNT sections between the Pd leads are 400, 6300, and 1200 nm, labeled A, B, and C, respectively. The tube diameter, measured by atomic force microscopy (AFM), is 3.0 ± 0.5 nm.

Each section can be biased in a field-effect transistor (FET) configuration, as shown in Fig. 1(a) for section A. An applied gate voltage shifts the Fermi energy from the gap region, where the FET is not conducting, into one of the 1D subbands of the CNT dispersion relation sketched in Fig. 2(b).

The conductance as a function of gate voltage for section A at two different temperatures is shown in Fig. 2(a). The threshold gate voltage at which the conductance starts to increase, $V_G \simeq 2$V, corresponds to the Fermi energy crossing the edge of the valence band. When the gate voltage is lowered, the Fermi energy is pushed further down into the valence band, where the dispersion relation is approximately linear, as shown in Fig. 2(b). Here the dispersion relation of the conduction (valence) bands are approximated by the relation

$$E(k) = +(-)\sqrt{(E_G/2)^2 + (\hbar v_F k)^2}, \quad (1)$$

where E_G and v_F are the carbon nanotube energy gap and Fermi velocity, respectively.[7] In this region of gate voltage, all three CNT field-effect transistors (from sections A, B, and C) show extremely high on-conductances $2.8G_0 < G_{ON} < 4G_0$ at 5 K. This indicates that all the sections are free from major defects and the contacts are highly transparent.[4,5,8–10]

When the temperature is lowered to temperatures T <10 K, conductance vs V_G shows large oscillation. The origin of these oscillations can be identified by measuring the conductance as a function of source-drain and gate voltages, clearly revealing that the oscillations are part of an interference

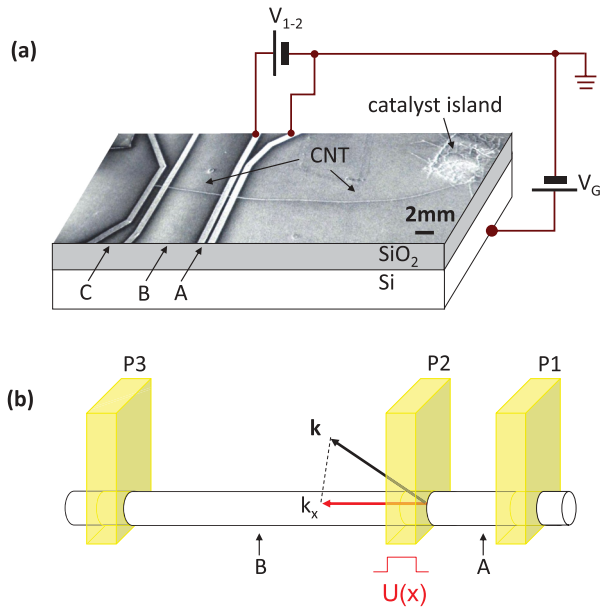

FIG. 1. (Color online) (a) Schematic diagram of the two-probe configuration measurement circuit combined with a scanning electron microscopy image of our sample. (b) Sketch of the CNT and palladium contacts showing the wave vector for charges propagating in device A and its component along the tube axis k_x.

pattern, as shown in Fig. 3. Here the color scale represents the differential conductance measured with a standard lock-in

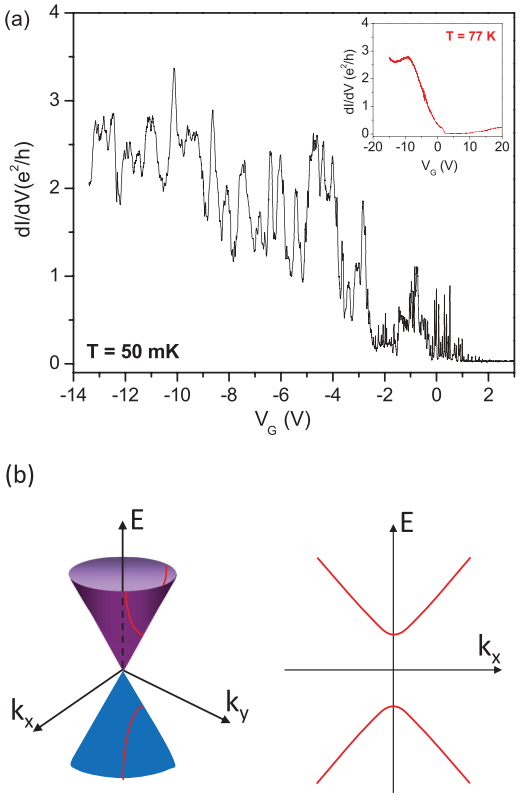

FIG. 2. (Color online) (a) Zero-bias differential conductance as a function of gate voltage for device A at two different temperatures. (b) Conduction and valence 1D subbands for a semiconducting carbon nanotube.

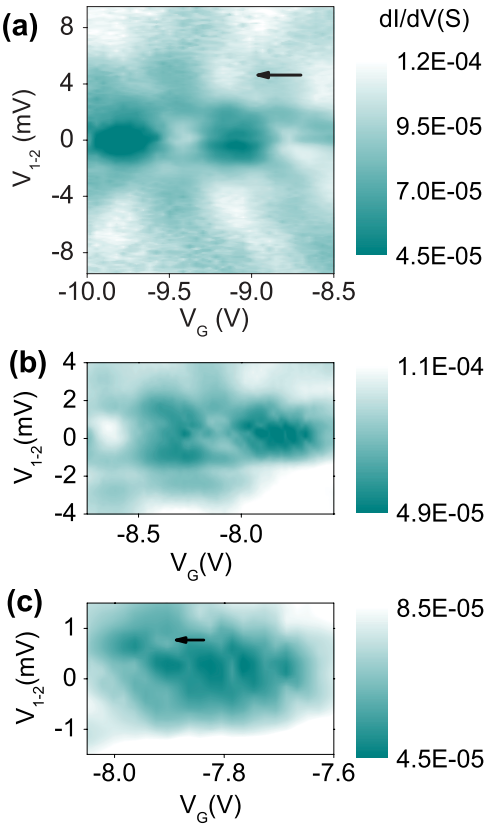

FIG. 3. (Color online) 2D plots of the differential conductance of device A as a function of source-drain voltage (V_{1-2}) and gate voltage (V_G) at T = 50 mK. (a) 2D plot in large gate and source-drain voltage ranges showing typical Fabry-Perot pattern with energy scale corresponding to the length of device A. (b) High-resolution 2D plot in a region close to zero source-drain voltage showing fine periodic structure of a Fabry-Perot pattern corresponding to a resonant length of more than 3 μm. (c) Enlargement of a region from (b).

technique. Similar patterns have been previously observed in both semiconducting and metallic carbon nanotubes with high-transparency contacts and they can be understood as Fabry-Perot resonances for the wave functions of electrons propagating in a carbon nanotube waveguide.[4,11]

Figure 3(a) shows a clear periodic pattern obtained in device A at 50 mK. Here the source-drain bias is connected to electrodes P1 and P2, whereas electrode P3 is not connected to the external circuit, as shown in Fig. 1(a). The maxima of differential conductance as a function of gate and source-drain voltages are due to the coherent interference of different electronic paths: In addition to the one-trip ballistic path, where electrons travel from one electrode P1 through the nanotube to the second electrode P2, there is a finite probability that electrons will be reflected at the contacts and will be captured by P2 only after a round trip in the nanotube. The condition for phase coherence of the two paths is satisfied for values of the wave vector

$$k_n = n\pi/L, \tag{2}$$

where n is an integer and $k_n 2L$ is the additional phase shift of the electronic wave function along the round trip, as in a Fabry-Perot resonator.

We can thus infer the length of the resonator by measuring the source-drain voltage corresponding to the first maximum in the Fabry-Perot pattern,[11]

$$e\Delta V_L = \Delta E = \hbar v_F \pi / L = (1.67\ \text{meV}\ \mu\text{m})/L, \quad (3)$$

where $\Delta E = E(k_{n+1}) - E(k_n)$, and we have used the linear approximation for the dispersion relation in Eq. (1). For device A, the value $V_{1-2} = \Delta V_L \simeq 4.5$ mV is indicated by the black arrow in Fig. 3(b) and corresponds to a bright spot where two (high-conductance) white lines cross, at the corner of one of the diamonds in the pattern. This value of ΔV_L corresponds to a length $L_A = 370$ nm, very close to the directly measured length of device A, 400 nm. Notably, the discrete values of electronic energies corresponding to resonances coincide with the energy spectrum of the carbon nanotube as a 1D quantum well with length $L = L_A$, because the same boundary conditions are applied.[12]

Figures 3(b) and 3(c) show high-resolution plots of the Fabry-Perot pattern obtained by zooming into a smaller region of gate and source-drain voltage. Here some fine features are distinguishable as new periodic structures within the Fabry-Perot pattern. These new structures are also Fabry-Perot patterns, but with a much smaller source-drain voltage spacing, with the first maximum at about 500 μV, corresponding to a Fabry-Perot resonator larger than 3 μm, about 10 times longer than the CNT section between electrodes P1 and P2 in device A.

III. DISCUSSION

A longer electronic path can only be obtained for electrons injected from the first electrode P1 and propagating across the second electrode P2 into the adjacent section of CNT, device B, and back into P2. Analogously to the experiment by Umbach *et al.*,[1] resonances occur when electrons following the longer path *outside the contact probes P1 and P2* are phase coherent with electrons propagating along the path in the short nanotube section A. We note that electrode P2 is wider than the charge-transfer length,[13,14] providing maximum transmission from the carbon nanotube to the Pd electrode. Even in this case, the transmission from the carbon nanotube to the Pd electrode is smaller than 1 and fine features due to nonlocal transport effects can still be measured. However, due to their small energy scale, they can only be clearly observed at low temperature (50 mK) and with high-resolution measurements of the two-dimensional (2D) Fabry-Perot patterns.

In Fig. 4 we test this explanation for the fine features of the pattern by applying a source-drain voltage to device B. We indicate the potential difference between electrodes P3 and P2 as V_{2-3}, and we set $V_{2-3} = -V_{1-2} + V_0$, as shown in Fig. 4(a). We then measure the differential conductance of device A as a function of the source-drain voltage V_{1-2}, at a fixed gate voltage, for different values of the offset V_0 [see Fig. 4(b)]. When $V_0 = 0$, $V_{2-3} = -V_{1-2}$ and the conductance of device A shows clear small Fabry-Perot oscillations around $V_{1-2} = 0$ mV that are superimposed onto the large Fabry-Perot oscillations. This is expected because Fabry-Perot oscillations are symmetric as a function of source-drain voltage; therefore a condition of constructive interference at a specific value of V_{1-2} will hold also at $-V_{1-2}$. When the offset $V_0 \neq 0$, then

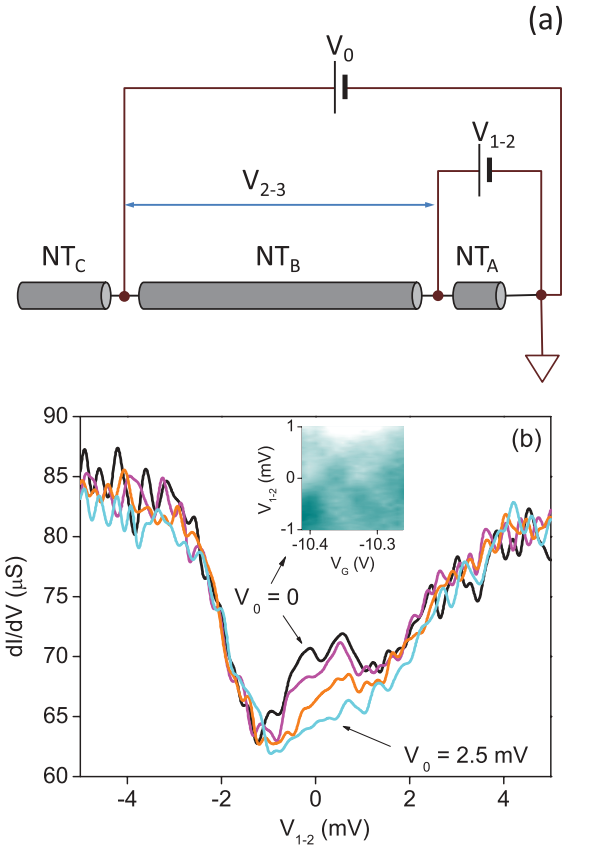

FIG. 4. (Color online) (a) Schematic of the equivalent biasing circuit for tuning the Fabry-Perot pattern with smaller energy scale. (b) Differential conductance of device A as a function of source-drain voltage (V_{1-2}) at $V_G = -10.07$ V and at T = 50 mK. Each curve is measured after changing the bias voltage across device B (see text), with $V_0 = 0$, 0.55, 1.53, and 2.55 mV. Inset: 2D plot of differential conductance for device A measured at $V_0 = 0$ showing the fine Fabry-Perot pattern.

$V_{2-3} \neq -V_{1-2}$, clearly disrupting the constructive interference of the small Fabry-Perot pattern. The small oscillations are then smeared out and eventually disappear, leaving only the large Fabry-Perot oscillations corresponding to $\Delta V_L \simeq 4.5$ mV. The bias voltage V_0 shifts the electrochemical potentials in the two adjacent CNT sections A and B with respect to each other. If $V_0 \neq 0$, the mismatch between the electron energies and momenta in sections A and B destroys the coherent pattern.

IV. MODELING AND SIMULATION

To obtain a detailed understanding of the picture presented in the previous section, we model the nanotube as a multiterminal conductor following the Landauer-Büttiker formalism,[15] with two sections A (short) and B (long) separated by a common electrode [P2 in Fig. 1(b)]. We assume that the contacts P1 and P2 for section A are symmetric and that the length of the adjacent section to the right of P1 is infinite. This is because the CNT section between P1 and the catalyst island is much longer than all the other sections, as shown in Fig. 1(a). We also assume that electrode P3 is at the same potential as the carbon nanotube, because it is electrically connected to it and

it is disconnected from the external circuit [see Fig. 1(a)]. We consider the "clean" limit, since in our experiment the electron mean free path is larger than the lengths of the nanotube sections; therefore no electron-impurity scattering is taken into account in our model.

The charge carriers propagating in section A towards P2 can either be reflected back into section A with probability R or transmitted with probability $T = 1 - R$. There are two different paths for transmission. In the first path charge carriers will be transmitted directly from the nanotube to the electrode P2. Here the CNT/Pd interface is modeled as a scatterer with transmission probability of 0.85. This is consistent with the high, nearly ideal conductance measured. In the second path, charge carriers will be transmitted along the axial CNT direction x into the adjacent section B.

Along the x path we assume that the Fermi level in the sections of nanotube covered by the electrodes is shifted from the Dirac point (corresponding to the middle of the bandgap for a semiconducting nanotube).[13,16] This shift is introduced in the model with the potential function $U(x)$, which is shaped as a square barrier [see Fig. 1(b)]. This barrier acts as a scatterer for electrons propogating along the carbon nanotube.

The physical origin of the Fermi-level shift is the interaction of the carbon nanotube with the metal forming the electrodes. Different work functions and, in some cases, chemical bonding cause charge transfer between the metal and the carbon nanotube, thereby shifting the Fermi level.

The width of $U(x)$ is set to 600 nm, equal to the width (L_c) of the electrode P2, whereas the height corresponds to the Fermi-level shift caused by the interaction with the metal. This shift cannot be readily predicted because it can vary substantially depending on the material work functions and the equilibrium distance between the carbon nanotube and the metal; therefore we adjusted it to match the experimental data by setting the barrier height equal to 2 meV, as discussed below. Furthermore, we assumed that the barrier height does not vary in the range of gate voltage considered in the simulations. This is because, when a gate voltage is applied, both the Fermi level in the uncovered nanotube and the Fermi level in the nanotube covered by the metal are shifted by the gate voltage, as shown in Ref. 13. For simplicity we assumed that the gate voltage shifts them by the same amount, keeping their relative shift caused by the interaction with the metal constant.

Charge carriers transmitted from section A to section B and then reflected by the electrode P3 will also have a finite probability to be captured by P2. Therefore, the two sections A and B can be considered as two 1D quantum wells that are coupled via the potential barrier $U(x)$ due to the common electrode P2. We account for this coupling using the Green's function method.[15] Electronic transport through this structure involves multiple transmission and reflection processes for the electron wave functions, which are solutions of the Dirac equation.[17–19] The transmission probability through the shallow barrier along the CNT axis depends on the electron energy E, on gate voltage V_G, and on the potential barrier profile $U(x)$. Interference effects, resonant scattering, and the barrier $U(x)$ will all affect the transmission probability $T_P(E,U,V_G)$ into the electrode P2. Relevant composition rules and calculation details of $T_P(E,U,V_G)$ can be found in earlier papers (see, e.g., Refs. 18 and 19).

The conductance $G = dI/dV_{1-2}$ of section A is computed by using the Landauer-Büttiker formula[15] for the electric current

$$I(V_G,V_{1-2}) = \frac{2e}{h}\int dE T_P(E,U,V_G)[n(E,T) - n(E - eV_{1-2},T)], \quad (4)$$

where $n(E,T)$ is the Fermi distribution function. In the simulations we considered a semiconducting CNT with diameter $d_T = 3$ nm, in agreement with the value measured by AFM. Following the experimental conditions, the Fermi level is shifted far away from the band edge, where the energy dispersion relation becomes approximately linear; therefore we found that the simulation results depend weakly on the CNT chirality. Temperature smearing effects are included in two ways: (i) via the distribution function $n(E,T)$ in Eq. (4) and (ii) via broadening of the quantized energy levels in the wells due to inelastic electron-phonon collisions with acoustic phonons. Although the electron-phonon scattering rate is very low (1 μeV at 4 K and 1 neV at 50 mK), it ensures that singularities of the density of states are rounded.

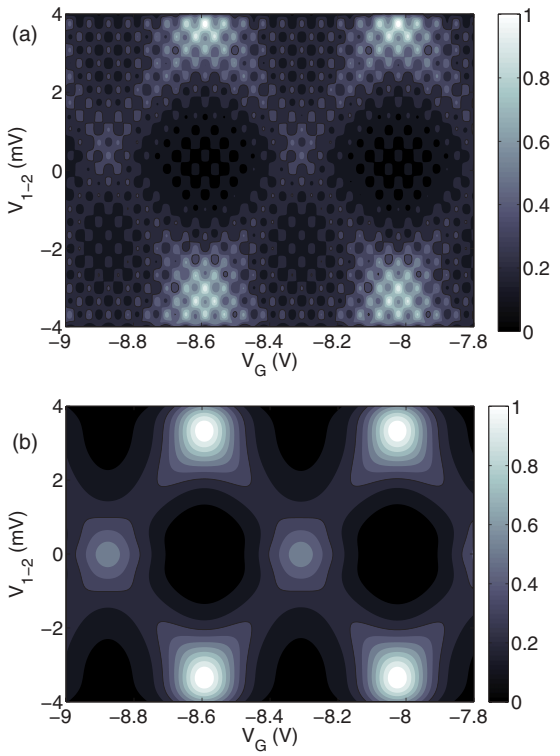

FIG. 5. (Color online) Calculated 2D plots of the conductance $G(V_G,V_{1-2})$ in units of $4G_0 = 4e^2/h$ at $T = 50$ mK. (a) Simulated 2D plot of the conductance of section A assuming the lengths of the short and long CNT sections to be $L_A = 440$ nm and $L_B = 4400$ nm, respectively. The two overlapping Fabry-Perot patterns are formed due to phase-coherent coupling of the electron states across the middle barrier. (b) The same plot for $G(V_G,V_{1-2})$, assuming L_B infinitely long.

In agreement with the experiment, the conductance of section A exhibits a remarkable new feature. In addition to the Fabry-Perot pattern with $e\Delta V_L^A = \hbar v_F \pi / L_A$, it contains an additional Fabry-Perot pattern with $e\Delta V_L^B = \pi \hbar v_F / L_B$, as shown in Fig. 5(a) (here $e\Delta V_L^B \simeq e\Delta V_L^A/10$). The additional pattern is due to coherent coupling between sections A and B through a wide potential barrier separating them.

Another feature clearly visible in the computed Fabry-Perot pattern is the stripe of reduced conductance $G(V_G, V_{1-2})$ which is parallel to the V_G axis and centered at $V_{1-2} = 0$. Within this stripe the features corresponding to the Fabry-Perot oscillations are darker than outside the stripe (the conductance maxima at $V_{1-2} = 4$ mV are brighter than the conductance maxima at $V_{1-2} = 0$). The stripe width, $\Delta V_{1-2} \simeq 4$ mV, centered at $V_{1-2} = 0$, is determined by the height of the potential barrier $U(x)$, because the higher conductance occurs for electronic energies larger than the barrier height. We set this height to 2 meV to match the experimental data, since a low-conductance stripe with width $\Delta V_{1-2} \simeq 4$ mV can be distinguished in the experimental plots [see Fig. 3(a)].

To provide further insight, we simulated the case where section B is infinitely long, leaving all the other parameters in the model unchanged. The result is the expected simple Fabry-Perot pattern with $e\Delta V_L^A = \hbar v_F \pi / L_A$, with no fine structure, as shown in Fig. 5(b).

V. CONCLUSION

Our experiments unambiguously show that, notwithstanding the large and strongly coupled Pd electrode, nonlocal effects are still present and charges can propagate phase coherently in the adjacent section. These nonlocal effects produce variation of conductance that can be as high as 13% for an electrode width that is 2 orders of magnitude larger than the nanotube diameter. This remarkably long range of coherence is explained by our theoretical analysis, where the Pd electrode creates a wide and shallow barrier. Electrons can propagate through such a wide, strongly coupled electrode without being scattered, on a ballistic phase-coherent path longer than 6 μm.

ACKNOWLEDGMENTS

The authors thank Joe Serene for fruitful discussions. This work was supported by the NSF (Grants DMR-0907220 and DMR-1008242). G.F. acknowledges financial support from the Russian Ministry of Science and Education (project 14.B37.21.1072) and the RFBR (Grant No. 10-02-92671-NNF-a).

*Current address: National Research Centre "Kurchatov Institute," Kurchatov sq. 1, Moscow, 123182, Russia.

†barbara@physics.georgetown.edu

‡Current address: MS 3B10, ATL Labs, Northrop Grumman, 1212 Winterson Road, Linthicum, MD 21090, USA.

[1] C. P. Umbach, P. Santhanam, C. van Haesendonch, and R. A. Webb, Appl. Phys. Lett. **50**, 1289 (1987).

[2] A. Makarovski, A. Zhukov, J. Liu, and G. Finkelstein, Phys. Rev. B **76**, 161405(R) (2007).

[3] G. Gunnarsson, J. Trbovic, and C. Schönenberger, Phys. Rev. B **77**, 201405(R) (2008).

[4] A. Javey, J. Guo, Q. Wang, M. Lundstrom, and H. Dai, Nature (London) **424**, 654 (2003).

[5] S. Ke, W. Yang, and H. U. Baranger, J. Chem. Phys. **124**, 181102 (2006).

[6] D. Mann, A. Javey, J. Kong, Q. Wang, and H. Dai, Nano Lett. **3**, 1541 (2003).

[7] M. J. Biercuk, S. Ilani, C. M. Marcus, and P. L. McEuen, *Carbon Nanotubes: Advanced Topics in the Synthesis, Structure, Properties and Applications*, edited by A. Iorio, G. Dresselhaus, and M. S. Dresselhaus, Topics in Appl. Physics, Vol. 111 (Springer, Heidelberg, 2008), pp. 455–493.

[8] J. Zhang, A. Tselev, Y. F. Yang, K. Hatton, P. Barbara, and S. Shafraniuk, Phys. Rev. B **74**, 155414 (2006).

[9] A. Tselev, Y. F. Yang, J. Zhang, P. Barbara, and S. E. Shafranjuk, Phys. Rev. B **80**, 054504 (2009).

[10] A. Tselev, K. Hatton, M. S. Fuhrer, M. Paranjape, and P. Barbara, Nanotechnology **15**, 1475 (2004).

[11] W. J. Liang, M. Bockrath, D. Bozovic, J. H. Hafner, M. Tinkham, and H. Park, Nature (London) **411**, 665 (2001).

[12] L. C. Venema, J. W. G. Wildoer, J. W. Janssen, S. J. Tans, H. L. J. Temminck Tuinstra, L. P. Kouwenhoven, and C. Dekker, Science **283**, 52 (1999).

[13] F. Xia, V. Perebeinos, Y. Lin, Y. Wu, and P. Avouris, Nat. Nanotechnol. **6**, 179 (2011).

[14] A. D. Franklin and Z. Chen, Nat. Nanotechnol. **5**, 858 (2010).

[15] S. Datta, *Electronic Transport in Mesoscopic Systems* (Cambridge University Press, Cambridge, UK, 1997).

[16] G. Giovannetti, P. A. Khomyakov, G. Brocks, V. M. Karpan, J. van den Brink, and P. J. Kelly, Phys. Rev. Lett. **101**, 026803 (2008).

[17] T. Ando, J. Phys. Soc. Jpn. **74**, 777 (2005).

[18] S. E. Shafranjuk, Europhys. Lett. **87**, 57007 (2009).

[19] S. E. Shafranjuk, Eur. Phys. J. B **80**, 379 (2011).